Title

Vagal Nerve Stimulation Reduces Ventricular Arrhythmias and Mitigates Adverse Neural Cardiac Remodeling Post-Myocardial Infarction.

Journal

JACC: Basic to Translational Science, 8(9)

Authors

Hadaya, Joseph
Dajani, Al-Hassan
Cha, Steven
et al.

Publication Date

2023-09-01

DOI

10.1016/j.jacbts.2023.03.025

Peer reviewed

JACC: BASIC TO TRANSLATIONAL SCIENCE VOL. 8, NO. 9, 2023

ORIGINAL RESEARCH - PRECLINICAL

Vagal Nerve Stimulation Reduces Ventricular Arrhythmias and Mitigates Adverse Neural Cardiac Remodeling Post–Myocardial Infarction

Joseph Hadaya, MD, PhD,[a,b] Al-Hassan Dajani, BS,[a] Steven Cha, BS,[a] Peter Hanna, MD, PhD,[a,b] Ronald Challita, MD,[a] Donald B. Hoover, PhD,[c,d] Olujimi A. Ajijola, MD, PhD,[a,b] Kalyanam Shivkumar, MD, PhD,[a,b] Jeffrey L. Ardell, PhD[a,b]

VISUAL ABSTRACT

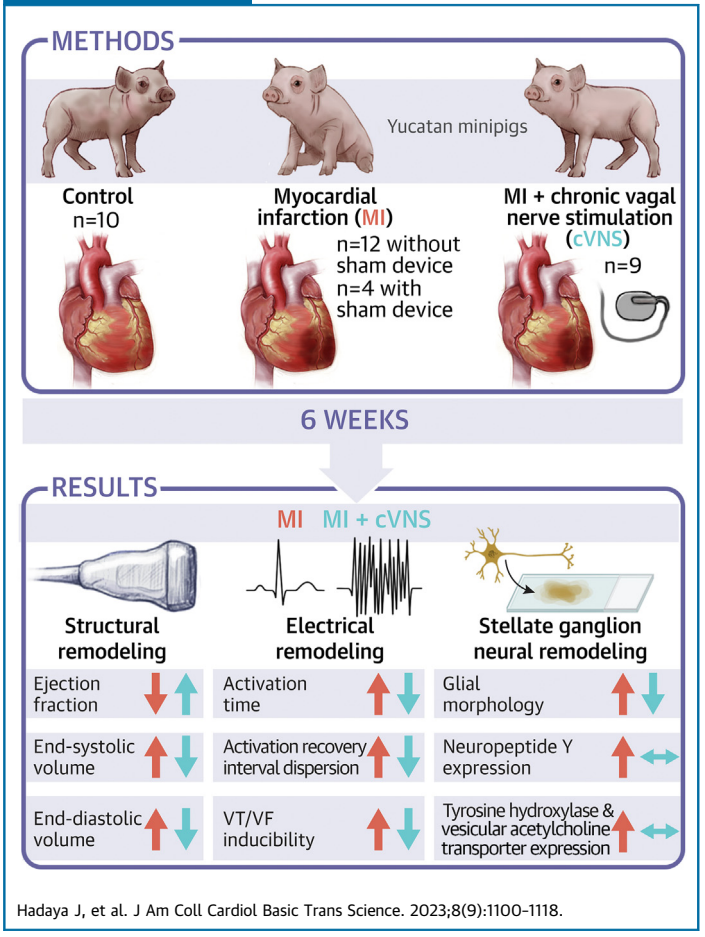

Hadaya J, et al. J Am Coll Cardiol Basic Trans Science. 2023;8(9):1100-1118.

HIGHLIGHTS

- **Vagal nerve stimulation has emerged as a promising therapeutic approach to combat the observed withdrawal of parasympathetic tone and to counteract the reflex-mediated sympathoexcitation associated with ischemic heart disease.**
- **Reactive cVNS, delivered in a neurophysiological-guided manner, resulted in a substantial improvement in cardiac mechanical function and dramatic reduction in ventricular arrhythmias in MI + cVNS pigs compared with MI pigs.**
- **cVNS stabilized MI-induced electrical heterogeneity in the scar-border zone, reduced anisotropic electrical propagation and conduction block, and normalized myocardial repolarization—key drivers of ventricular arrhythmias in vivo.**
- **cVNS reduced aberrant structural remodeling of the scar-border zone and principal sympathetic efferent and afferent ganglia (stellate and T1 dorsal root ganglia).**
- **cVNS preserved sympathetic control of the heart after MI.**

ISSN 2452-302X https://doi.org/10.1016/j.jacbts.2023.03.025

SUMMARY

This study sought to evaluate the impact of chronic vagal nerve stimulation (cVNS) on cardiac and extracardiac neural structure/function after myocardial infarction (MI). Groups were control, MI, and MI + cVNS; cVNS was started 2 days post-MI. Terminal experiments were performed 6 weeks post-MI. MI impaired left ventricular mechanical function, evoked anisotropic electrical conduction, increased susceptibility to ventricular tachycardia and fibrillation, and altered neuronal and glial phenotypes in the stellate and dorsal root ganglia, including glial activation. cVNS improved cardiac mechanical function and reduced ventricular tachycardia/ventricular fibrillation post-MI, partly by stabilizing activation/repolarization in the border zone. MI-associated extracardiac neural remodeling, particularly glial activation, was mitigated with cVNS. (J Am Coll Cardiol Basic Trans Science 2023;8:1100–1118)

ABBREVIATIONS AND ACRONYMS

APD = action potential duration

ARI = activation recovery interval

BSS = bilateral sympathetic chain stimulation

CGRP = calcitonin gene-related peptide

cVNS = chronic vagal nerve stimulation

DRG = dorsal root ganglia

EF = ejection fraction

GFAP = glial fibrillary acidic protein

LAD = left anterior descending

LV = left ventricular

MI = myocardial infarction

nNOS = neuronal nitric oxide synthase

NPY = neuropeptide Y

NSVT = nonsustained ventricular tachycardia

PBS = phosphate-buffered saline

PES = programmed electrical stimulation

PGP9.5 = protein gene product 9.5

ROI = regions of interest

RT_{90} = repolarization time at 90% repolarization

SCD = sudden cardiac death

TH = tyrosine hydroxylase

VA = ventricular arrhythmia

VAChT = vesicular acetylcholine transporter

VF = ventricular fibrillation

VNS = vagal nerve stimulation

VT = ventricular tachycardia

Myocardial infarction (MI) and sudden cardiac death (SCD) are the leading cause of mortality worldwide.[1,2] Neurohormonal remodeling after MI is characterized by chronic sympatho-excitation, which, although initially helping to maintain cardiac output, ultimately becomes maladaptive and contributes to the risk of death.[3,4] Coronary reperfusion, antiadrenergic therapy, and neurohormonal blockade have drastically reduced mortality after MI, but such therapies remain inadequate in preventing disease progression and SCD.[5,6]

Parasympathetic dysfunction has been increasingly recognized as a causal driver of adverse cardiac remodeling and ventricular arrhythmias (VAs) after MI.[7-9] Clinically, interest in the antiarrhythmic actions of the parasympathetic nervous system dates to 1977, whereby increased vagal drive was demonstrated to terminate ventricular tachycardia.[10] In animal models, chronic vagal nerve stimulation (cVNS) reduces myocardial injury and improves cardiac function in small mammals, but has not been reproducibly evaluated in higher-level organisms, limiting its applicability.[11-15] Moreover, the translatability of chronic VNS for cardiovascular disease has been hampered by a lack of knowledge regarding cardiac reflexes, cardiac and extracardiac remodeling that occurs during disease, and appropriate delivery of VNS therapy. In fact, the 3 major existing clinical trials for ccVNS for heart failure each targeted different neural substrates and delivered therapy at vastly different stimulation parameters, with only 1 trial reporting improvements in left ventricular (LV) function.[16-19]

Efficacy of bioelectric interventions depend on the site of delivery, the stimulation protocol used, and the substrate on which the neuromodulation is acting, both neural and end-organ target.[20] Our laboratory has previously characterized the neural fulcrum, a balance point for delivery of VNS whereby both afferent and efferent arms of the parasympathetic system are engaged, producing a null heart rate response.[21] In a guinea pig model of pressure overload, we have previously found that cVNS, delivered at the neural fulcrum, improved LV function by reducing myocyte apoptosis and hypertrophy.[22] Similarly, in a guinea pig model of MI, cVNS improved LV systolic function by stabilizing myocardial metabolism and intrinsic cardiac neuronal function.[12] Although prior work identifies several cardioprotective mechanisms of cVNS, studies in large mammals are imperative to evaluate the translational potential of cVNS in the treatment of cardiac

From the [a]UCLA Cardiac Arrhythmia Center and Neurocardiology Research Program of Excellence, David Geffen School of Medicine at UCLA, Los Angeles, California, USA; [b]Molecular, Cellular, and Integrative Physiology Program, University of California, Los Angeles, Los Angeles, California, USA; [c]Department of Biomedical Sciences, Quillen College of Medicine, East Tennessee State University, Johnson City, Tennessee, USA; and the [d]Center of Excellence in Inflammation, Infectious Disease and Immunity, East Tennessee State University, Johnson City, Tennessee, USA.

The authors attest they are in compliance with human studies committees and animal welfare regulations of the authors' institutions and Food and Drug Administration guidelines, including patient consent where appropriate. For more information, visit the Author Center.

Manuscript received January 3, 2023; revised manuscript received March 29, 2023, accepted March 29, 2023.

JACC: BASIC TO TRANSLATIONAL SCIENCE VOL. 8, NO. 9, 2023
SEPTEMBER 2023:1100–1118

dysfunction after acute MI. Moreover, the antiarrhythmic actions of cVNS post-MI remain unknown.

Herein, we studied how cVNS mitigates myocardial structural and neural remodeling as well as ventricular arrhythmogenesis after MI. We used a clinically relevant model, the Yucatan minipig, which recapitulates many features of human ischemic cardiomyopathy including SCD. We delivered VNS therapy in a neuroscience-guided manner, targeting the neural fulcrum using telemetry in the conscious state. We evaluated minipigs in 3 groups: control, untreated MI (a subset of which received sham VNS therapy), and cVNS + MI.

METHODS

STUDY OVERVIEW AND APPROVAL. Animal experiments were approved by the UCLA Institutional Animal Care and Use Committee and performed in accordance with the National Institutes of Health's Guide for the Care and Use of Laboratory Animals. A total of 41 Yucatan minipigs (*Sus scrofa*, S&S Farms) of both sexes, weighing 50 to 60 kg at terminal experiment, were used for the present study. Six animals died within 48 hours of MI from SCD, and were not included in final analysis. Surviving animals comprised 3 experimental groups: control (n = 10), MI (n = 12 without sham VNS; n = 4 with sham VNS), and MI + cVNS (n = 9). At the end of terminal experiments, animals were euthanized in concordance with Institutional Animal Care and Use Committee guidelines. **Figure 1** presents overall study design and methods used in this project.

IMPLANTATION OF VAGAL NERVE STIMULATORS. After sedation with midazolam (1 mg/kg, intramuscular) and ketamine (10 mg/kg, intramuscular), animals were endotracheally intubated and mechanically ventilated (tidal volume 300 to 450 mL, rate 10 to 12 breaths/min). Anesthesia was maintained with isoflurane (1%-4%, inhaled), and carprofen (4.4 mg/kg, intramuscular) and buprenorphine (0.02 mg/kg, intramuscular) were administered for analgesia. Ceftiofur (4 mg/kg, intravenous) and cefazolin (1 mg) were administered for perioperative antibiotic prophylaxis. Ear veins and the right or left femoral artery or tail artery were cannulated for medication administration and invasive blood pressure monitoring. Three-lead electrocardiogram, oxygen saturation, and end-tidal carbon dioxide were monitored. Body temperature was maintained using a forced-air normothermia system, and 0.9% NaCl (5-6 mL/kg/h) was administered to replenish insensible fluid loses. The intended incision site over the right ventral neck was anesthetized with a 1:1 mixture of lidocaine (1 mg/kg) and bupivacaine (1 mg/kg). The right external jugular vein and right vagus nerve were exposed. A wireless telemetry device (M01-F1, Data Sciences International) was implanted with 1 lead fluoroscopically guided to the cavo-atrial junction through the right external jugular vein, and the second lead tunneled to a pocket in the lateral neck. A bipolar VNS cuff (PerenniaFLEX Model 304, LivaNova) was placed around the right cervical vagus nerve and attached to a VNS pulse generator (Vitaria Model 7103, LivaNova). VNS devices were tested intraoperatively for evoked bradycardia to confirm device placement. Devices and leads were secured with 4-0 polypropylene sutures to the adjacent fascia, and the fascia overlying the vagus nerve and external jugular vein were each closed separately with absorbable suture. The device pockets and incision were then closed with 4 layers of absorbable suture, and the animals were extubated and recovered. Carprofen (4.4 mg/kg, once daily) was administered for 3 days for postoperative analgesia. Pigs were evaluated twice daily for 10 days, and daily thereafter.

TITRATION OF VNS THERAPY. To achieve therapeutic levels of VNS, stimulation settings were systematically titrated to those that produced a null heart rate change at 5 Hz frequency and 250 μs pulse width during the on phase of VNS (14 seconds on, 66 seconds off) as shown in Supplemental Figure 1A. To accomplish this, titration was began at 5 Hz, 130 μs, and 0.25 mA. At each titration session, current was increased in 0.25-mA increments until side effects (cough, gastrointestinal upset) were elicited; current was then decreased by 0.25 mA and the pig rested for >1 day at these settings. Once a current of 3 mA was achieved, pulse width was stepped up to 250 μs and a similar process was repeated. Low-intensity stimulation (>1.5 mA) usually results in tachycardia (Supplemental Figure 1B); at higher-intensity stimulation bradycardia is evoked. Neural fulcrum was defined as a null change in heart rate during on-phase VNS, and titration was discontinued once fulcrum was achieved. In the MI + cVNS group, 2 days after MI, VNS was restarted and maintained at 5 Hz, 250 μs, and 17.5% duty cycle (14 seconds on, 66 seconds off), with intensity as previously determined individually to achieve neural fulcrum and maintained as such until termination.

MYOCARDIAL INFARCTION. For induction of MI, the same anesthesia, analgesia, and monitoring protocol described already in this article was performed. The right or left femoral artery was accessed using the modified Seldinger technique and a vascular access sheath was placed. VA prophylaxis consisted of

FIGURE 1 Study Design and Methods

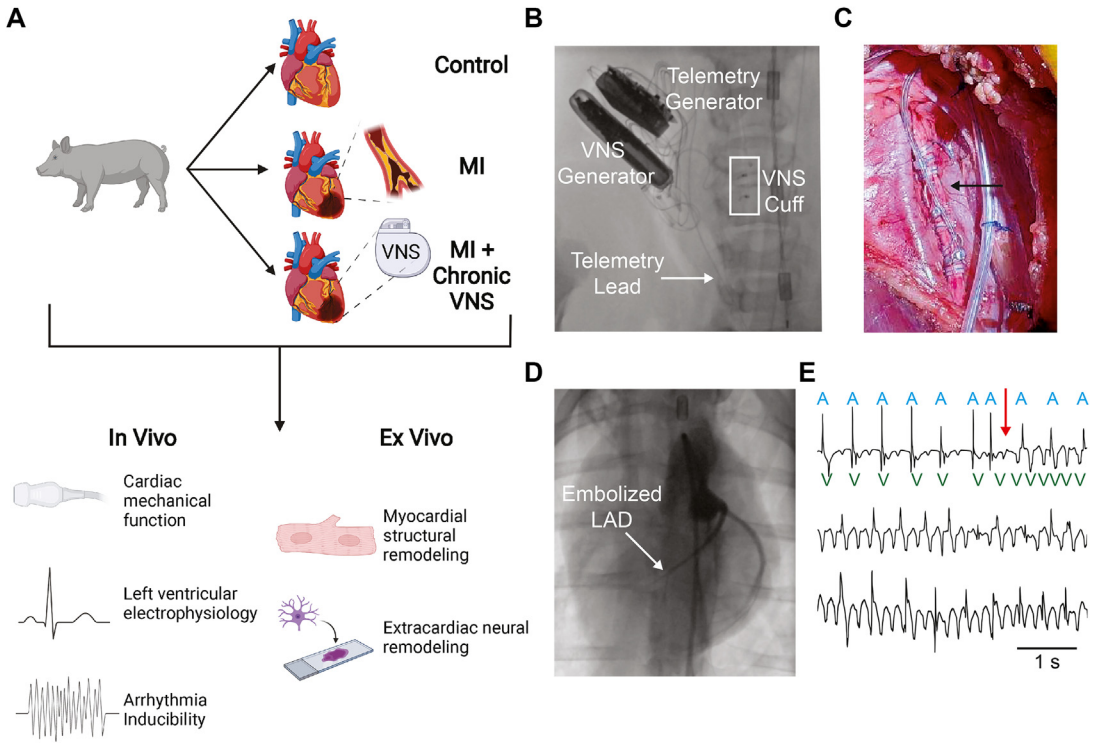

(A) Control, MI, and MI + cVNS Yucatan minipigs underwent in vivo and ex vivo evaluation of cardiac mechanical and electrophysiological function, as well as myocardial and extracardiac neural remodeling. **(B and C)** Representative images of implanted VNS generator at the right vagus nerve. **(D)** Left coronary angiogram after microsphere embolization of the mid-LAD coronary artery. **(E)** Spontaneous VT in an ambulatory pig observed 2 days after MI, which led to sudden death. Atrial depolarization **(near field)** annotated as **A**, and ventricular depolarization **(far field)** annotated as **V**; note maintenance of native atrial rhythm during VT. Scale bar: 1 s. Figure partly created using BioRender.com. cVNS = chronic vagal nerve stimulation; LAD = left anterior descending coronary artery; MI = myocardial infarction; VNS = vagal nerve stimulation; VT = ventricular tachycardia.

amiodarone (1.5 mg/kg, intramuscular) and lidocaine (2 mg/kg, intravenous), whereas periprocedural anticoagulation was maintained with heparin (5,000 U, intravenous). Under fluoroscopic guidance, an AL1.0 guide catheter (Medtronic) and 0.014-inch guidewire (Balance Middleweight Universal, Abbott) were used to cannulate the left coronary artery. An angioplasty balloon catheter was advanced over the guidewire to the mid-left anterior descending (LAD) coronary artery to the level of the second diagonal branch and inflated. A suspension (2.25 mL diluted to 6 mL with 0.9% NaCl) of polysterene microspheres (Polysciences Inc.) was used to embolize the distal LAD coronary artery. Hyperacute T waves, T-wave inversion, or ST-segment elevation were evident on surface electrocardiogram. External cardioversion and standard cardiopulmonary resuscitation were performed if the animal developed unstable ventricular tachycardia (VT) or ventricular fibrillation (VF). For animals requiring cardiopulmonary resuscitation, epinephrine (0.01 mg/kg, intravenous) was administered every 3 to 5 minutes, and amiodarone (1.5 mg/kg, intravenous) and lidocaine (2 mg/kg, intravenous) re-administered one additional time. Animals were extubated and recovered as already described. All pigs received carprofen (4.4 mg/kg) daily for 2 days and, if defibrillation was required, buprenorphine (0.02 mg/kg, intravenous) was administered twice daily for 2 days.

SURGICAL PREPARATION AT TERMINAL STUDY. Pigs were sedated, intubated, mechanically ventilated,

maintained on isoflurane, and monitored as already described. Tiletamine-zolazepam (4-6 mg/kg, intramuscular) was used for induction and fentanyl citrate (20 mg/kg, intravenous) was administered for analgesia. Vascular access sheaths were placed in bilateral femoral arteries and veins for administration of fluids, monitoring, and placement of intracardiac catheters. Arterial blood gas contents were also evaluated hourly and ventilation parameters adjusted or sodium bicarbonate administered as needed to ensure physiological parameters for experimental studies. The thorax and heart were exposed through a median sternotomy. A pericardial cradle was created to support the heart. The parietal pleural was divided posteriorly and the sympathetic chain isolated at the level of the stellate ganglia. The left vagus was dissected as already described, and the right vagus lead was disconnected from the pulse generator. After completion of surgical procedures, anesthesia was transitioned from isoflurane to alpha-chloralose (25-50 mg/kg/h, intravenous), an anesthetic that does not depress cardiac and autonomic reflexes.

NERVE STIMULATION. Bipolar platinum nerve cuffs (Microprobes) were placed around the right and left sympathetic chain at the level of the stellate ganglia. A bipolar VNS cuff was placed around the left vagus as already described. Nerve stimulation was performed using a Grass S88 stimulator, interfaced through a PSIU6 photoelectric constant-current isolation unit (Grass Instruments). For sympathetic chain stimulation, threshold was defined as the current required to elicit a 10% increase in heart rate or LV end-systolic pressure at a fixed frequency of 4 Hz and fixed pulse width of 4 ms. For VNS, stimulus threshold was defined as the current required to elicit a 10% change in heart rate at a fixed frequency of 10 Hz and fixed pulse width of 1 ms. Bilateral sympathetic chain stimulation (BSS) was performed at 1.5 times threshold at moderate (4 Hz) and high (10 Hz) intensity to evaluate evoked sympathetic responses. To test whether acute VNS influenced induction of VT or VF, acute bilateral VNS was performed in conjunction with VA inducibility at 1.5 times fulcrum (right) or threshold (left) intensity.

ECHOCARDIOGRAPHY. Echocardiography was performed as previously described.[23] LV ejection fraction was calculated using the modified Simpson method. LV wall thicknesses were measured in diastole.

HEMODYNAMIC AND ELECTROPHYSIOLOGICAL DATA ACQUISITION AND ANALYSIS. A solid-state pressure catheter (Mikro-Tip Model SPR-350, Millar Instruments) was placed in the left ventricle through the femoral artery and used to measure rate of change of LV pressure (dP/dt) and heart rate. A lead II electrocardiogram and bipolar electrocardiograms were measured with surface electrodes and quadripolar or duodecapolar electrode catheter (Boston Scientific). These data were acquired, digitized, and analyzed offline using a data acquisition system (Cambridge Electronics Design Power1401 and Spike2). LV contractility or systolic function was evaluated with the maximum rate of change of LV pressure (LV dP/dt_{max}) while lusitropy was evaluated using the minimum rate of change of LV pressure (LV dP/dt_{min}).

A custom, 128-electrode thin film array (NeuroNexus) was placed over the left ventricle scar-border zone (or equivalent area in controls) to acquire unipolar epicardial electrograms. Data was sampled at 1,380 Hz using an AlphaLab SnR acquisition system (Alpha Omega). Activation recovery intervals (ARIs) were analyzed from each epicardial electrogram using Scaldyn (University of Utah) as previously described.[24] Maps were plotted using Fiji[25] with identical scaling and bilinear interpolation for the 3 experimental groups simultaneously. Activation time was identified as the time from the beginning to the minimum dV/dt in the activation wavefront and recovery time by the maximum dV/dt of the repolarization wavefront. Activation delay was defined as the maximum minus minimum repolarization time, whereas activation dispersion was assessed as the variance of activation times. Repolarization time at 90% repolarization (RT_{90}) was defined as the 95th percentile minus the 5th percentile of local repolarization times as previously described.[26] Repolarization gradient was defined as the RT_{90} divided by the geometric distance between corresponding electrodes. ARI was calculated as the difference between recovery time and activation time, and ARI dispersion as the variance in ARI. ARI serves as a strong in vivo surrogate for local action potential duration.[27]

ARRHYTHMIA INDUCIBILITY. VA inducibility was performed using programmed electrical stimulation (PES) using a Micropace EPS 320 cardiac stimulator (Micropace EP) interfaced with a Prucka CardioLab System (GE Healthcare). PES was performed at a stimulus train (S1) 20% faster than the resting heart rate followed by an S2 extrastimulus with a 10 ms decrement until 200 ms or until effective refractory period was reached. If the first extrastimulus did not induce sustained VT or VF, a second (S3) extrastimulus was added and the decrement process repeated. This was performed through a third (S4) extrastimulus. For animals receiving cVNS therapy, PES was performed twice: without acute VNS, and with bilateral acute VNS for 30 min before and during

PES. Animals that did not experience sustained VT or VF for >30 seconds with 3 extrastimuli were considered noninducible. Nonsustained ventricular tachycardia (NSVT) was defined as at least 3 or more ventricular beats at a rate of >120 beats/min that terminated within 30 seconds. Animals were classified as noninducible, induced for NSVT, or induced for sustained VT/VF. An arrhythmogenicity index was calculated to quantify the ease of VT/VF inducibility based on the stimulus drive train and number of extrastimuli as previously described.[23] Higher values indicate greater ease of inducibility.

TISSUE COLLECTION AND PROCESSING. The LV anterior myocardium adjacent to the LAD coronary artery (consisting of scar, border, and remote regions), right stellate ganglia, and first thoracic dorsal root ganglia (DRG) were collected and rinsed in cold phosphate-buffered saline (PBS). Myocardial samples were fixed in 10% formalin (Sigma-Aldrich) at room temperature for 72 hours, washed with PBS 4 times for 1 hour each, and preserved in 70% ethanol. Stellate and DRG were fixed in 4% paraformaldehyde (Electron Microscopy Sciences) at 4°C for 24 hours, washed with PBS 4 times for 1 hour each, and preserved in PBS with 0.02% sodium azide.

Masson's trichrome staining was performed on LV samples spanning the scar-border zone, just adjacent to the LAD, and evaluated for structural abnormalities. Abnormalities included increased myocytolysis, decreased staining for muscle bands, reactive hypertrophy, and presence of dysmorphic myocytes. The following arbitrary scale was used: 3 = very abundant, 2 = moderate, 1 = low, and 0 = none or rare. Three to four sections were evaluated per animal, and values were recorded for subepicardium, midwall, and subendocardium. These were added on the first pass and an average value for each animal was calculated.

Stellate ganglia sections were stained using a 2-day protocol with the following combinations: 1) protein gene product 9.5 (PGP9.5), tyrosine hydroxylase (TH), vesicular acetylcholine transporter (VAChT); 2) PGP9.5, TH, neuropeptide Y (NPY); and 3) PGP9.5, glial fibrillary acidic protein (GFAP), S100 Calcium Binding Protein B (S100B). The right stellate ganglia were paraffin embedded to acquire 5-μm sections along the long-axis of the ganglia. Slides with paraffin-embedded sections underwent 2 consecutive, 10-minute baths in xylene. Slides were then placed in ethanol baths of varying concentrations (100% for 10 min, followed by 95% for 5 minutes, followed by 70% for 5 minutes). Finally, slides were placed in dH_2O for 5 minutes. Slides were placed in an antigen unmasking solution, which was made by diluting 2.5 mL of antigen retrieval buffer in 250 mL of dH_2O and boiling to 90°C, for 25 minutes, then cooled for 1 hour. Slides were then placed in a soaking buffer solution (PBS with 0.4% TX-100) for 30 minutes at 4°C. Tissue wells were created on slides using a hydrophobic barrier pen and 50 to 100 μL PBS was added to each well depending on tissue size. The slides were placed in a humidified chamber and agitated for 5 minutes. PBS was then replaced with blocking buffer solution (PBS + 10% donkey serum with 0.1% TX-100) for 1 hour. Primary antibody solution was then made by adding primary antibodies (Supplemental Table 1) to the blocking buffer solution, which replaced the blocking solution in the wells. Slides were agitated overnight at 4°C. Slides were then warmed to room temperature and washed with PBS with 0.2% TX-100 3 times. Secondary antibody solution was then made by adding secondary antibodies (Supplemental Table 2) to the blocking buffer solution, which then replaced the primary antibody solution in each well. Slides were agitated gently for 1 hour at room temperature then washed 3 times with PBS. PBS was then replaced with refractive index matching solution that covered each section entirely and cover slips were placed directly after to secure the tissue. Slides were imaged using confocal microscopy.

DRG were stained using a 7-day protocol with the following combinations: 1) PGP9.5, calcitonin gene-related peptide (CGRP), neuronal nitric oxide synthase (nNOS); and 2) PGP9.5, GFAP, S100B. The right first thoracic DRG from each subject was embedded in agarose to acquire 100-μm sections along the long-axis of the ganglia. Each section was placed in 1 mL of blocking solution containing 10% donkey serum, 0.2% Triton X-100, and PBS for overnight incubation with slight agitation. A primary antibody solution was made using blocking solution and primary antibodies (Supplemental Table 1). After 3 nights of incubation with slight agitation, the sections were washed with PBS every hour for at least 6 washes. A secondary antibody solution was made with blocking solution and secondary antibodies (Supplemental Table 2). Sections were incubated for 3 nights with slight agitation. Sections were then washed with PBS every hour for at least 6 washes. Sections were mounted on slides and refractive index matching solution was added in drops until the sections were covered entirely, and a coverslip was placed to secure the tissue. Slides were imaged using confocal microscopy.

Confocal imaging was performed using a Zeiss LSM-880 confocal laser microscope (Zeiss). The

following lasers were used: 488 (Green), 562/Cy3 (Red), and 647 (Blue). Imaging was done at 10x and stitched together using the tile scan feature. Maximum intensity projections for a representative Z-stack were subsequently used for analysis.

Three representative 500- × 500-μm regions of interest (ROI) were selected for each stellate section on Zen Black (Zeiss). Sixteen-bit full-resolution images were exported and analyzed on ImageJ Software (National Institutes of Health). The PGP9.5, TH, and VAChT combination was analyzed for cholinergic transdifferentiation by using the cell counter feature in ImageJ to obtain a total cell count using the PGP9.5 channel and a count of cells double-labeled for TH and VAChT. The PGP 9.5, TH, and NPY combination was similarly analyzed for NPY expression. Glial analysis was performed by selecting 15 satellite glial cells (5 cells per ROI) from each animal for individual analysis. The length and area of each satellite glial cell was measured on ImageJ using the GFAP stain. The immunoreactive area (μm^2) per cell for each ROI was calculated by converting the GFAP channels to binary images. The thresholding tool in ImageJ was then used to calculate the total GFAP stain area in each ROI. A ratio of total GFAP area to total cell count based on the PGP9.5 channel was then calculated for each ROI and averaged for each animal.

One representative 500- × 500-μm ROI was selected for each DRG section. Sixteen-bit full-resolution images were exported and analyzed on ImageJ Software. The PGP9.5, CGRP, and nNOS staining combination was analyzed for cells labeled for nNOS or CGRP and PGP9.5. To evaluate glial activation, the immunoreactive area (μm^2) per cell for each ROI was similarly calculated by converting the GFAP channels to binary images. The thresholding tool was then used to calculate the total GFAP stain area in each ROI. A ratio of total GFAP area to total cell count based on the PGP9.5 channel was then calculated for each animal.

STATISTICAL ANALYSIS. Data are presented as mean ± SEM. Normality was assessed using the Shapiro-Wilk test. For normally distributed variables, differences in SD were tested using the Brown-Forsythe test. For normally distributed variables, comparisons were made using standard analysis of variance if SDs were not significantly different, and Welch's analysis of variance if SDs differed. For non-normally distributed variables, the Kruskal-Wallis test was used. Pairwise comparisons were subsequently performed using the *t* test or Wilcoxon rank-sum test, and the 2-stage step-up method of Benjamini, Krieger, and Yekuteili was used to control for multiple comparisons. For comparisons between solely 2 groups, the *t* test or Wilcoxon rank-sum test was used. Categorical variables were studied using the chi-square test. A 2-sided *P* value of <0.05 was deemed statistically significant. Statistical analysis was conducted using Prism 9 (GraphPad Software).

RESULTS

IMPLEMENTATION OF cVNS IN YUCATAN MINIPIGS. To study the effects of cVNS on MI (**Figure 1A**), we developed a strategy for cVNS delivery at the neural fulcrum.[21] Our preliminary studies suggested that titration to therapeutic VNS parameters required approximately 30 days to prevent side effects in pigs. Because the majority of myocardial remodeling occurs within the first month after MI, we implanted right vagus nerve cuffs, pulse generators, and telemetry units and titrated to therapeutic settings before MI (Supplemental Figure 1). This strategy allowed us to begin therapeutic VNS on-demand after MI. Both MI + cVNS pigs and MI + sham cVNS pigs underwent VNS pulse generator and lead implantation, followed by titration to VNS fulcrum (~4 weeks). Once VNS fulcrum was achieved (5 Hz, 250 μs, mean current 1.8 ± 0.2 mA), therapy was discontinued and pigs underwent MI at least 1 day after cessation of therapy to ensure no memory effect from VNS titration.[28] MI was induced in MI, MI + sham cVNS, and MI + cVNS pigs using percutaneous embolization of the LAD coronary artery, and infarcts were allowed to mature for 6 to 8 weeks before terminal study. VNS therapy was restarted 2 days after MI in the MI + cVNS group. Among all animals undergoing MI induction, 6 experienced SCD within 2 days of MI, confirming the adequacy of this model. A sensitivity analysis, reported later in this article, found no significant difference in sympathetic function, electrophysiological parameters, cardiac structural remodeling, or arrhythmia inducibility in MI compared with MI + sham cVNS groups (Supplemental Figure 2). As such, these were considered as one group for the primary analysis reported in this study. Age- and weight-matched controls that had not undergone any interventions were used for comparison.

cVNS RESCUES CARDIAC MECHANICAL FUNCTION AFTER MI. To determine whether chronic VNS influences basal LV contractile function after MI, we performed echocardiography in controls, MI, and MI + cVNS animals (**Figure 2A**). MI animals had significant impairments in LV systolic function compared with controls, with LV ejection fraction (EF) of 40.6% ± 1.2% compared with 71.6% ± 0.4%

FIGURE 2 cVNS Improves Cardiac Mechanical Performance and Contributes to Greater Cardiac Sympathetic Reserve Post-MI

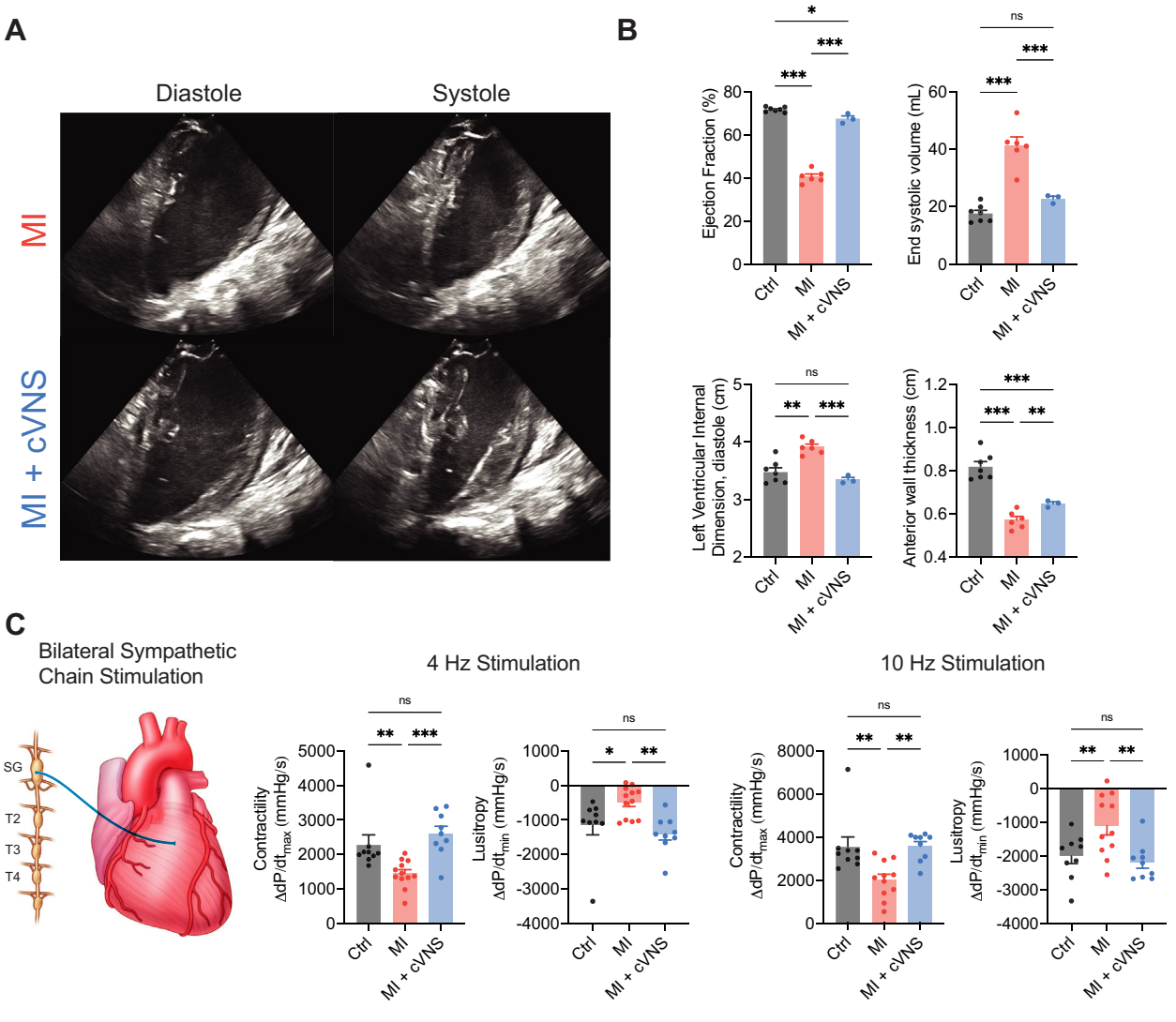

(A) Representative long-axis echocardiograms of MI and MI + cVNS animals. Note the degree of chamber dilation and greater end-systolic volume in MI compared with MI + cVNS. **(B)** MI resulted in a significant reduction in LV systolic function, with lower ejection fraction and higher LV internal dimension in diastole, which was ameliorated using cVNS. **(C)** MI animals had impaired inotropic (dP/dt_{max}) and lusitropic (dP/dt_{min}) sympathetic responses to both 4 Hz and 10 Hz bilateral sympathetic chain stimulation, which was rescued using cVNS. Data presented as mean ± SEM and analyzed using ANOVA and *t* test. *$P < 0.05$; **$P < 0.01$; ***$P < 0.001$. ANOVA = analysis of variance; Ctrl = control; LV = left ventricular; other abbreviations as in Figure 1.

($P < 0.001$). Chronic VNS therapy rescued changes in EF to 67.4% ± 1.3%, although this remained significantly different from controls (Figure 2B). Similarly, MI resulted in greater LV end-systolic volumes and LV internal diameter in diastole, which were significantly improved in MI + cVNS animals. Wall thickness in the anterior wall, the LV region primarily perfused by the LAD, significantly decreased in MI vs control animals (0.82 ± 0.02 cm vs 0.57 ± 0.04 cm; $P < 0.001$), which was partially attenuated with cVNS therapy to 0.65 ± 0.01 cm (Figure 2B). The myocardial regions not perfused by the LAD remained unaffected (data not shown). To evaluate functional sympathetic control of the heart, we performed BSS and tested whether MI or MI + cVNS influenced changes in inotropy or lusitropy. Baseline hemodynamics and thresholds used for sympathetic nerve stimulation are reported in Supplemental Tables 3 and 4. MI resulted in dysfunctional inotropic and lusitropic responses to BSS, which were restored to levels

FIGURE 3 Antiarrhythmic Effects of cVNS

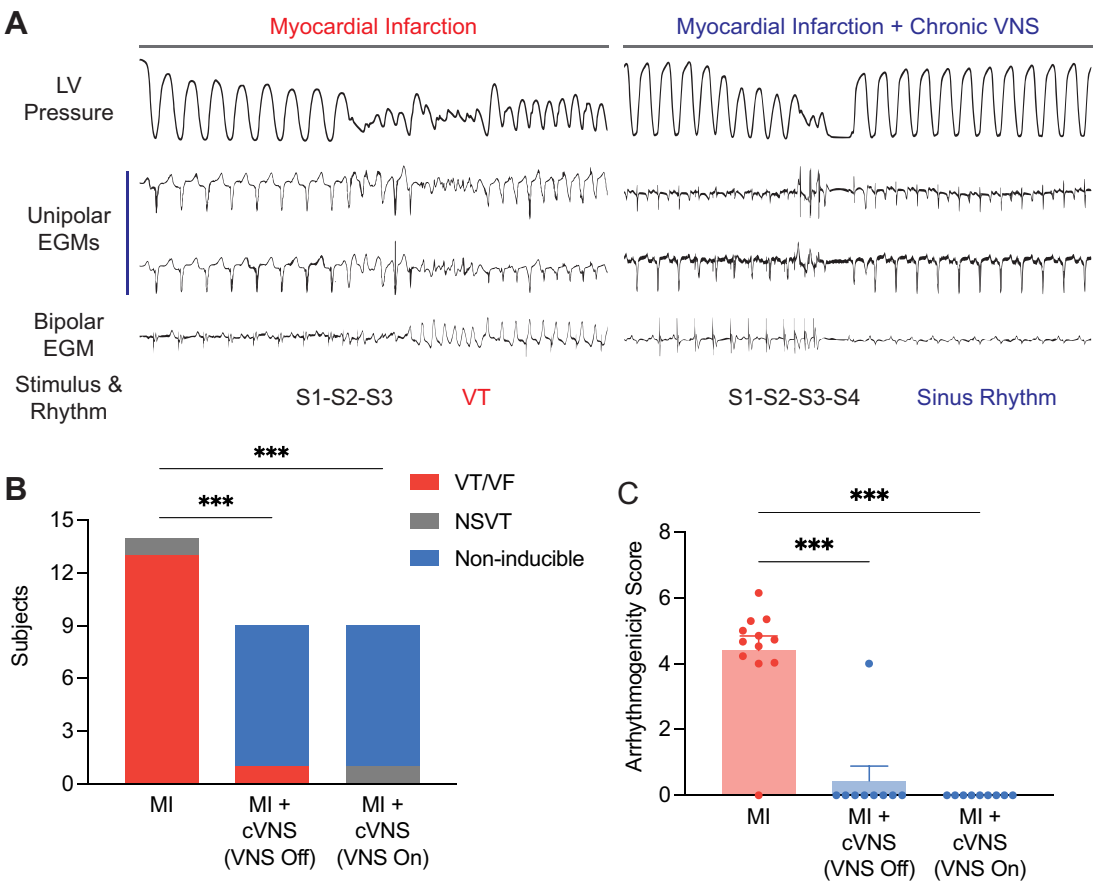

(A) Representative LV pressure tracing, and unipolar and bipolar EGMs during programmed electrical stimulation in MI and MI + cVNS animal. **(B)** cVNS significantly reduced the inducibility of sustained VT or VF regardless of whether PES was performed with or without active VNS. **(C)** MI animals demonstrated significantly greater ease of VT/VF induction compared with MI + cVNS pigs. Data presented as count **(B)** or mean ± SEM **(C)** and analyzed using chi-square test **(B)** or Kruskal-Wallis and Wilcoxon rank-sum test **(C)**. *$P < 0.05$; **$P < 0.01$; ***$P < 0.001$. EGM = electrogram; NSVT = nonsustained ventricular tachycardia; PES = programmed electrical stimulation; VF = ventricular fibrillation; other abbreviations as in Figures 1 and 2.

similar to controls in MI pigs receiving cVNS therapy (Figure 2C). This was evident with both moderate- and high-intensity stimulation, suggesting that cVNS ameliorated reduced cardiac sympathetic reserve evident in MI animals.

cVNS REDUCES THE SUSCEPTIBILITY TO VAs AFTER MI. MI and its associated structural abnormalities in the border zone are known to increase the risk of life-threatening VAs. To evaluate whether cVNS reduces VAs after MI, we performed PES using extrastimulus pacing in MI and MI + cVNS pigs. A representative recording of VT induction is shown in Figure 3A; as noted, the MI animal was induced with 2 extrastimuli, whereas the MI + cVNS subject remained non-inducible despite 3 extrastimuli. VT or VF was induced in 92% of MI pigs, whereas the remaining animal experienced NSVT (Figure 3B). In MI + cVNS subjects, 11% were inducible for VT/VF at baseline ($P < 0.001$ vs MI), whereas the remaining were non-inducible (Figure 3B). When active VNS was re-established in MI + cVNS pigs for 30 minutes before and during the extrastimulus protocol, 0% were inducible for VT/VF and 11% experienced NSVT ($P < 0.001$ vs MI) (Figure 3B). The ease of inducibility, quantified based on the rate of the drive train and number of extrastimuli required to induce VT/VF, was significantly greater in MI compared with MI + cVNS subjects (4.4 vs 0.4; $P < 0.001$) but similar regardless of whether active VNS therapy was applied (Figure 3C).

VNS EXERTS ANTIARRHYTHMIC EFFECTS IN PART VIA STABILIZATION OF CARDIAC ELECTROPHYSIOLOGICAL

FIGURE 4 cVNS Stabilizes Electrical Activation Across the Infarcted Left Ventricle, Mitigates Conduction Block, and Promotes Homogeneous Activation in Sinus Rhythm

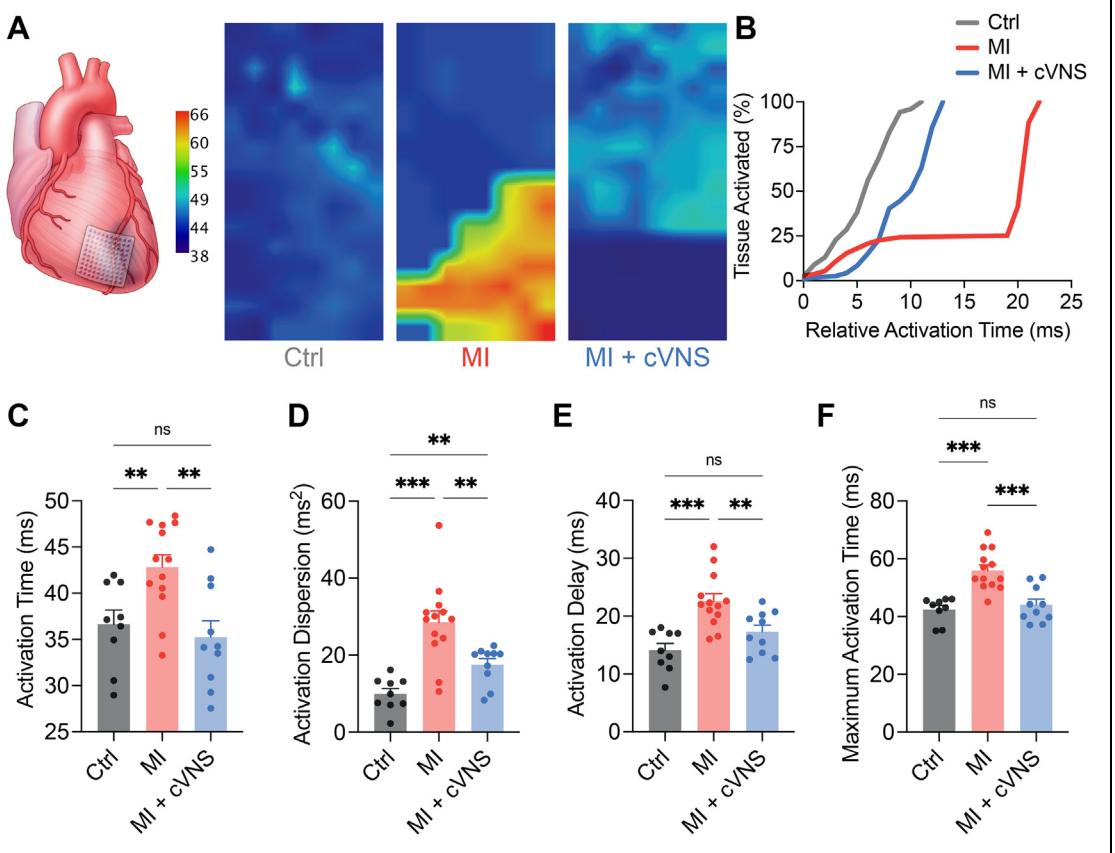

(A) High-density electrophysiological mapping was performed across the LV scar-border zone (and equivalent region in control), representative activation maps for control, MI, and MI + cVNS displayed. **(B)** Representative tissue activation curve demonstrating isotropic conduction in control animals compared with anisotropic conduction with block in MI, which was qualitatively improved with cVNS. **(C to F)** MI animals displayed significantly worse activation properties in sinus rhythm including greater activation time, dispersion, delay, and maximum activation time. These were all normalized in MI + cVNS animals, except activation dispersion **(D)**. Data presented as mean ± SEM and analyzed using ANOVA or Welch's ANOVA and *t* test. *$P < 0.05$; **$P < 0.01$; ***$P < 0.001$. Abbreviations as in Figures 1 and 2.

FUNCTION. To evaluate the substrate-level mechanisms by which cVNS ameliorated VAs, we performed high-resolution electrical mapping of the LV scar-border zone in MI and MI + cVNS animals, and corresponding anatomic region in controls. Heterogeneous areas of myocardial scars contribute to ventricular arrhythmogenesis by facilitating slow conduction and re-entry. These regions, as well as subsets with late tissue activation, are the clinical targets of catheter ablation, the current standard of care for re-entrant VAs. Figure 4A demonstrates representative activation maps for control, MI, and MI + cVNS animals. As quantified in Figure 4B, MI animals displayed substantial conduction block (ie, no increase in proportion of LV tissue activated relative to time) compared with controls, which was qualitatively improved with cVNS therapy. Consistent with prior work, we found that MI quantitatively resulted in greater mean ventricular activation time, activation dispersion (variance of activation time), activation delay, and maximal activation time (Figures 4C to 4F). Chronic VNS therapy normalized the majority of these measures to levels comparable with controls, including mean activation time, delay, and maximal activation time, whereas activation dispersion, a sensitive measure for scar, was improved relative to MI (17.6 ± 1.5 ms^2 vs 28.5 ± 2.9 ms^2; $P = 0.008$) but remained greater than control (17.6 ± 1.5 ms^2 vs 10.0 ± 1.4 ms^2; $P = 0.001$; Figure 4D). These findings suggest that cVNS

FIGURE 5 cVNS Reduces Repolarization Heterogeneity and Leads to More Shallow Repolarization Gradients

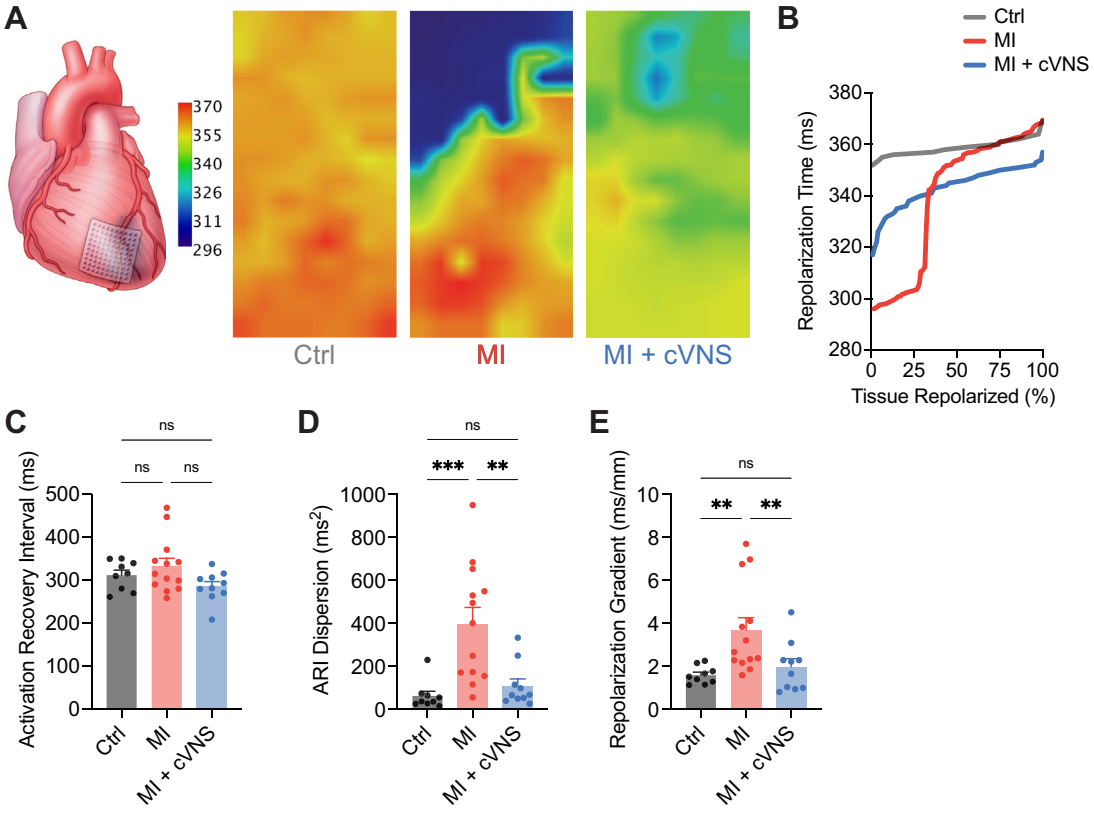

(A) Representative repolarization maps for control, MI, and MI + cVNS demonstrating very steep and heterogeneous repolarization across the scar-border zone in MI animals, which was qualitatively improved in MI + cVNS. **(B)** Representative tissue repolarization curve demonstrating regions of rapid changes in repolarization time in a MI animal. **(C)** No significant difference in LV ARI was evident in the studied groups, whereas MI resulted in greater ARI heterogeneity, which was partially improved with cVNS **(D)**. Repolarization gradients **(E)** were significantly greater in MI animals, and normalized with cVNS. Data presented as mean ± SEM and analyzed using Welch's ANOVA and *t* test **(C)** or Kruskal-Wallis and Wilcoxon rank-sum test **(D and E)**. *$P < 0.05$; **$P < 0.01$; ***$P < 0.001$. ARI = activation recovery interval; other abbreviations as in Figures 1 and 2.

substantially remodels myocardial scars and ameliorates the majority of the conduction abnormalities observed after MI.

Abnormal myocardial repolarization properties, particularly heterogeneity, have been implicated in arrhythmias after MI. Representative repolarization maps and repolarization times for each study group are shown in Figures 5A and 5B. To study the influence of cVNS on repolarization properties after MI, we first quantified LV ARI, a surrogate measure for action potential duration (APD) that can be readily measured in vivo without causing myocardial injury.[27] Interestingly, we found no significant difference in mean ARI across the scar-border zone, or equivalent region, in control compared with MI and MI + cVNS animals (Figure 5C). To evaluate heterogeneity in ARI, we examined ARI dispersion, and found that MI induced substantial increases in ARI dispersion (399 ± 75 ms^2 vs 63 ± 22 ms^2; $P < 0.001$), which were normalized using cVNS therapy (110 ± 32 ms^2) (Figure 5D). Because differences in ARI may be related to differences in activation dynamics, we tested whether differences in repolarization time persisted across the scar-border zone by evaluating differences in the 95th relative to 5th percentile of repolarization time (RT_{90}). MI resulted in substantially greater differences in RT_{90} across the mapped region relative to control, which was ameliorated with cVNS therapy (Figure 5E). Steep repolarization gradients have recently been associated with the development or maintenance of re-entrant arrhythmias.[5,29,30] As anticipated, MI pigs had steep repolarization gradients compared with controls (3.7 ± 0.6 ms/mm vs 1.6 ± 0.1 ms/mm; $P = 0.007$), which was similarly

FIGURE 6 cVNS Mitigates Structural Remodeling at the Scar-Border Zone

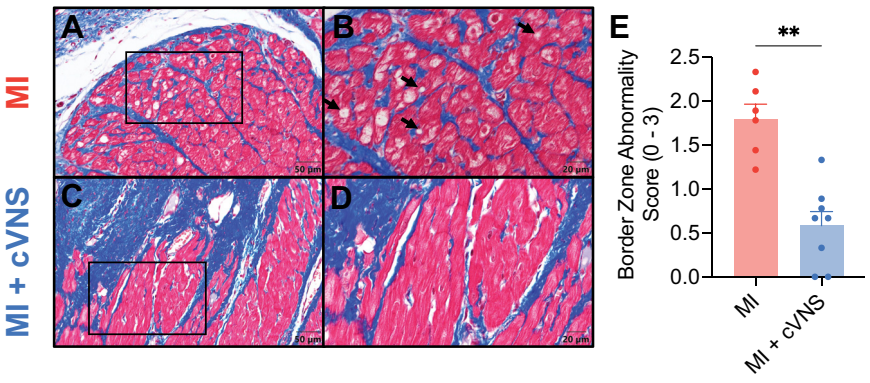

Representative Masson's trichrome stains from MI **(A, inset, B)** and MI + cVNS **(C, inset, D)** animals. MI animals more commonly had myocytolysis **(arrow)**, hypertrophy, and decreased muscle band staining. which was less common in MI + cVNS animals **(D, E)**. Data presented as mean ± SEM and analyzed using Wilcoxon rank-sum test. *$P < 0.05$; **$P < 0.01$; ***$P < 0.001$. Abbreviations as in Figure 1.

improved with cVNS therapy (2.0 ± 0.4 ms/mm) (Figure 5E). Taken together, these findings strongly suggest that cVNS not only improves conduction across the infarcted myocardium, but improves the repolarization properties of myocytes themselves in vivo, protecting the heart against VAs.

cVNS EXERTS ITS ANTIARRHYTHMIC EFFECT PARTLY BY REDUCING ABERRANT REMODELING OF THE MYOCARDIAL SUBSTRATE. Given the observed improvement in mechanical and electrophysiological properties of cVNS in infarcted hearts, we evaluated structural changes in the scar-border zone. We performed Masson's trichrome staining on LV sections spanning the scar-border zone, just adjacent to the site of LAD embolization. Compared with MI animals (Figures 6A and 6B), we qualitatively observed less myocytolysis, improved staining of muscle bands, less reactive hypertrophy, and more transmural scar in cVNS + MI pigs (Figures 6C and 6D). These specific findings, particularly a reduction in myocytolysis (Figure 6A, arrows), is consistent with reduced potential for VT/VF. Quantification revealed a marked reduction in border zone abnormality among MI + cVNS compared with MI animals (1.8 ± 0.2 vs 0.6 ± 0.2; $P = 0.001$; Figure 6E).

MI ALTERS NEURAL AND GLIAL PHENOTYPES IN THE PERIPHERAL NERVOUS SYSTEM, WHICH ARE PARTLY ATTENUATED WITH cVNS. In both humans and animal models, myocardial injury leads to extracardiac neural remodeling, which may drive sympatho-excitation after MI.[31,32] Stellate ganglia surgically removed from patients with recurrent VT showed evidence of oxidative stress, glial activation, and changes in neuronal phenotypes.[32] To evaluate for changes in neuronal phenotypes in our porcine models, we colabeled stellate ganglia for: 1) PGP9.5 (a pan-neuronal marker), TH, and VAChT; and 2) PGP9.5 and NPY. We found a significant increase in TH+/VAChT+ neurons after MI, which was unchanged with cVNS therapy (Figure 7A). Similarly, the proportion of NPY+ neurons significantly increased after MI, a change that trended toward normalization with cVNS (Figure 7B). To evaluate for glial activation, stellate ganglia were colabeled with S100B, GFAP, and PGP9.5. MI resulted in a substantial increase in glial activation, as evaluated by glial area and glial area relative to neurons per section, which was reversed to control levels with cVNS treatment (Figure 7C). Similar findings were evident on evaluation of length, width, and thickness of glial cells in the stellate, whereas no difference was found in neuronal cell size (Supplemental Figure 3).

We similarly evaluated changes in afferent neuronal phenotypes and glial activation in the first thoracic DRG, the primary source of general visceral fibers that innervate the heart. nNOS expression significantly increased after MI, which was mitigated using cVNS (Figure 8A). The expression of CGRP was similar in the 3 study groups (Figure 8B). Consistent with the stellate, MI led to significantly increased glial activation in the DRG, which was ameliorated using cVNS (Figure 8C). There was no significant difference in overall neuron size, nNOS + neuron size, or CGRP + neuron size by study group (data not shown).

FIGURE 7 cVNS Reduces Extracardiac Neural Remodeling in the Stellate Ganglia

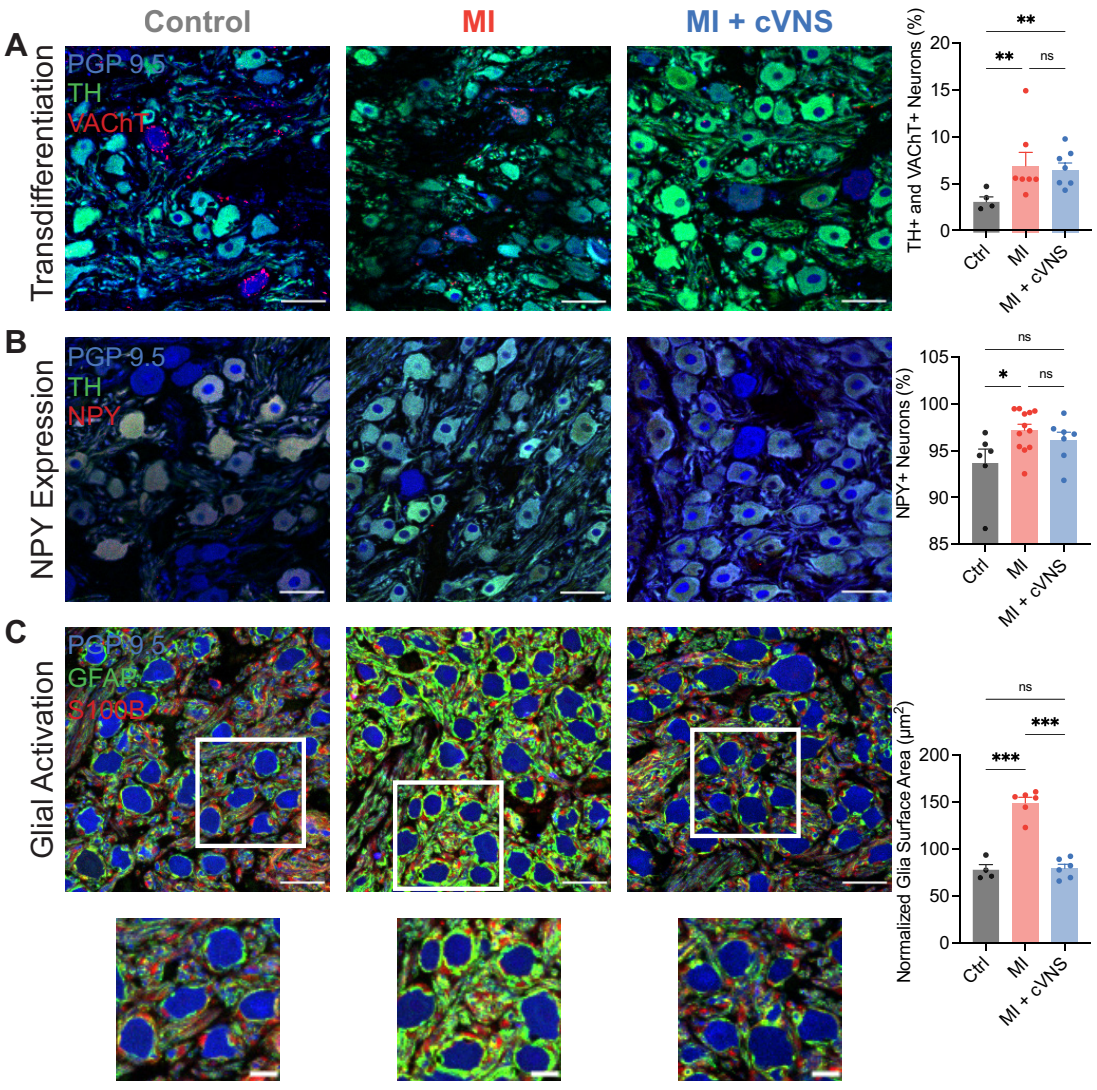

(A) Cholinergic transdifferentiation occurred after MI in both MI and MI + cVNS groups, and was unaffected by cVNS therapy. **(B)** Expression of NPY in the stellate ganglia was greater in MI animals compared with control, but similar in MI + cVNS pigs relative to control. **(C)** Glial activation significantly increased in MI animals compared with controls, which was ameliorated in MI + cVNS. Scale bar: 50 μm (except insets scale bar: 20 μm). Data presented as mean ± SEM and analyzed using Kruskal-Wallis and Wilcoxon rank-sum test **(A and B)** or Welch's ANOVA and *t* test **(C)**. *$P < 0.05$; **$P < 0.01$; ***$P < 0.001$. GFAP = glial fibrillatory acidic protein; NPY = neuropeptide Y; PGP9.5 = protein gene product 9.5; S100B = S100 calcium-binding protein B; TH = tyrosine hydroxylase; VAChT = vesicular acetylcholine transporter; other abbreviations as in Figures 1 and 2.

DISCUSSION

In this work, we demonstrated a substantial improvement in cardiac mechanical function and dramatic reduction in VAs in MI + cVNS pigs compared with MI pigs. We established that cVNS stabilized MI-induced electrical heterogeneity in the scar-border zone, reduced anisotropic electrical propagation and conduction block, and normalized myocardial repolarization—key drivers of VAs in vivo. We demonstrated that cVNS reduced aberrant structural remodeling of the scar-border zone and

FIGURE 8 cVNS Reduces Glial Activation After MI in the Thoracic Dorsal Root Ganglia

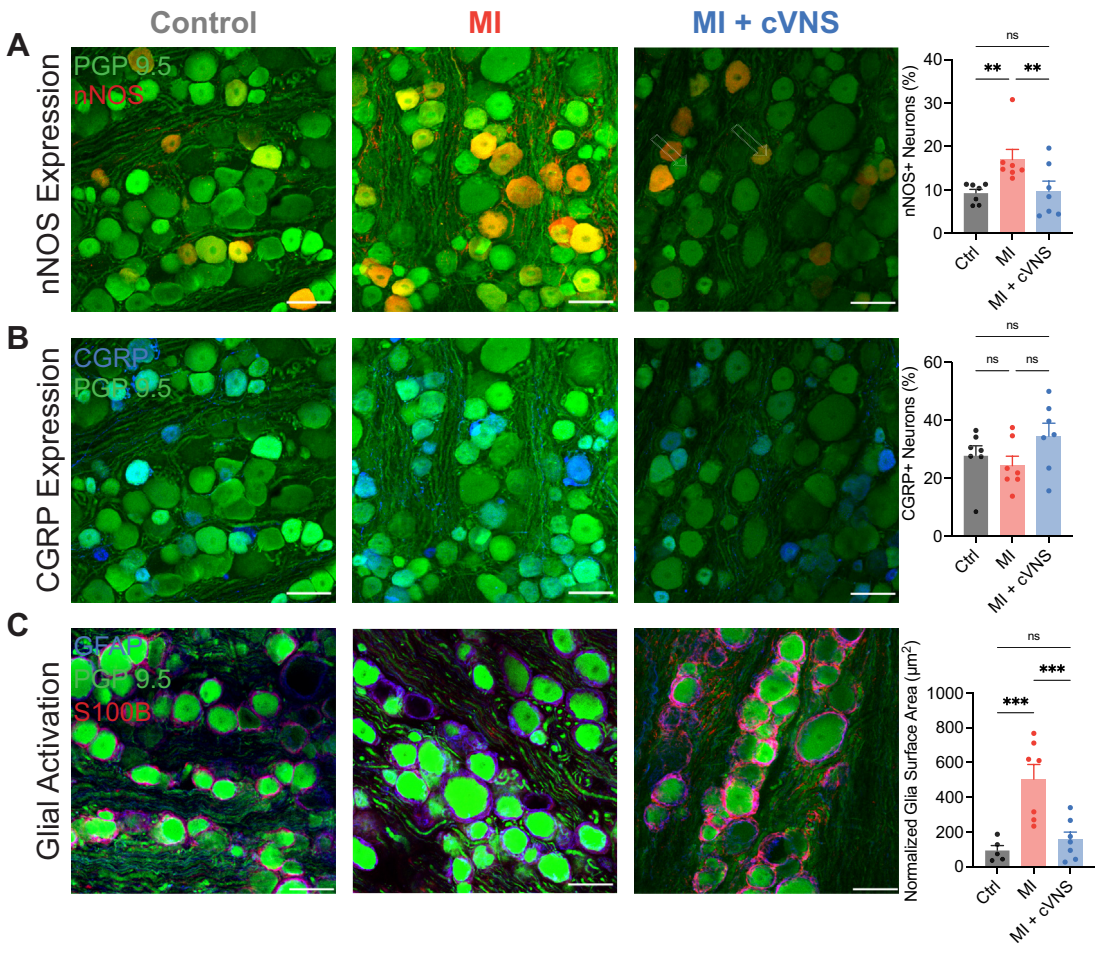

(A) nNOS expression significantly increased after MI, which was mitigated using cVNS. **(B)** No difference was evident in CGRP expression across study groups. **(C)** MI resulted in significantly greater glial activation in the thoracic dorsal root ganglia, which was significantly reduced in MI + cVNS animals. Scale bar: 50 μm. Data presented as mean ± SEM and analyzed using Kruskal-Wallis and Wilcoxon rank-sum test. *$P < 0.05$; **$P < 0.01$; ***$P < 0.001$. CGRP = calcitonin gene-related peptide; nNOS = neuronal nitric oxide synthase; other abbreviations as in Figures 1, 2, and 7.

principal sympathetic efferent and afferent ganglia (stellate and T1 DRG). Finally, cVNS preserved sympathetic control of the heart after MI.

Although acute VNS has been well studied in the setting of acute ischemia or MI, there is a paucity of studies evaluating the impact of cVNS on cardiac function, arrhythmias, and remodeling after MI, particularly in large mammals. Among canines with healed anterior MI, acute VNS initiated within 15 seconds of coronary occlusion reduced VAs, although these effects were partly attenuated by atrial pacing to control for a 75 beats/min bradycardia.[33] Similarly, the antiarrhythmic effects of acute VNS in ischemia-reperfusion injury in a porcine model were mitigated by administration of atropine and were not evident when VNS was started during reperfusion, suggesting that the acute cardioprotective effects are mediated by muscarinic receptors.[34,35] In the present study, we found that cVNS resulted in favorable myocardial and neural remodeling that prevented the induction of VT or VF. This antiarrhythmic effect was evident even in the absence of acute VNS, suggesting that its effects are not mediated solely by acute activation of muscarinic receptors. In guinea pigs, our group has previously found that chronic VNS, started 10 days after MI, significantly improved myocardial contractile function.[12] In the present study, we similarly found cVNS to improve LV systolic function,

with near normalization of EF to controls. This is consistent with prior work whereby VNS, delivered either conventionally or via optogenetic approaches, improved ventricular function in mice when initiated 48 hours postinfarction.[13,36] In our study, we found that control and MI + VNS animals had greater sympathetic reserve using electrical stimulation of the sympathetic chain because these groups of animals were able to more effectively mount inotropic and lusitropic responses compared with MI pigs. These specific findings indicate that cVNS may ameliorate abnormal calcium handling and inefficient excitation-contraction coupling that occurs in MI and heart failure. Consistent with this notion, Machhada et al[36] demonstrated that optogenetic stimulation of vagal pre-ganglionic neurons improved exercise capacity in rats with MI-induced heart failure. Structurally, cVNS reduced thinning of the anterior wall of the left ventricle, the primary location of MI in this model. Consistent with its antiarrhythmic effect, VNS reduced the degree of myocytolysis and dysmorphic myocytes in the scar-border zone, and qualitatively resulted in more homogeneous scars, which clinically are known to be less arrhythmogenic.[37,38] To our knowledge, this represents the first systematic evaluation of reactive VNS therapy on cardiac mechanical function, structural remodeling, and arrhythmias in large mammals, and is a logical step to translation of VNS therapy to clinical applications.

MI results in formation of areas of slow activation or conduction, and transient or permanent unidirectional block, such that steep APD differences manifest over relatively short distances. Moreover, in our model, we found that MI alters basic electrophysiological properties of border zone myocytes, promoting spontaneous activity. These cellular and tissue-level phenomenon act in concert to promote VA risk. This risk was particularly elevated in our model, as all but 1 MI animals were induced for sustained monomorphic VT or VF at terminal study, and 6 died acutely after MI. Although prior work suggests that acute VNS reduces ischemia-induced arrhythmias in canines, limited data exist regarding the impact of cVNS on induction of VAs and mechanisms of arrhythmogenesis.[33,39] Notably, MI + cVNS animals were equally protected from VT or VF when inducibility was performed with or without active VNS therapy, suggesting that the observed cardioprotective effects are likely mediated by changes in the myocardial and neural substrate. This finding may be related to the strong antiarrhythmic effect observed with cVNS in our model, limiting our power to identify an additional effect of acute VNS superimposed on cVNS treatment post-MI in our VT inducibility assessment. We found that cVNS improves conduction across the scar-border zone, which is consistent with studies demonstrating that VNS preserves connexin-43 expression in the setting of acute ischemia in small mammals.[11] The effects of VNS were not limited to electrical propagation because VNS also positively influenced myocyte excitability and repolarization properties. Scar-border zone myocardium from MI + cVNS pigs had significantly less myocytolysis, a highly arrhythmogenic component of infarcted human myocardium.[38] Moreover, in vivo, MI + cVNS animals demonstrated less ARI dispersion and more shallow repolarization gradients across the scar-border zone. These changes in electrophysiological properties of the myocardium warrant further study at the cellular and molecular level.

Acute myocardial injury leads to abnormal cardiac afferent signaling to both the stellate ganglia and high-thoracic DRG, ultimately resulting in amplified sympathetic drive.[7,40,41] Consistent with this notion, stellate ganglia from humans with ischemic cardiomyopathy, as well as in animal models, are characterized by oxidative stress, glial activation, and changes in neuronal phenotypes.[31,32,42] In the present work, stellate ganglia neuronal and non-neuronal cells displayed marked changes after MI, including glial activation and cholinergic transdifferentiation. Cholinergic transdifferentiation, a process whereby cardiac sympathetic neurons transition to an acetylcholine-producing phenotype in the setting of heart failure or after MI, has been shown to reduce APD heterogeneity in small mammals and may be an adaptive physiological response to injury.[43-45] Because one central premise of neuromodulation is to stabilize imbalance among the cardiac nervous system, we evaluated whether these changes were altered with cVNS therapy. We found that cholinergic transdifferentiation remained prominent and unchanged after cVNS therapy, whereas glial cell activation substantially decreased compared with MI animals. This finding underscores the importance of non-neuronal populations in extracardiac ganglia as potential avenues for further study and therapeutic targets. These non-neuronal populations are heterogeneous, and modify neuronal function through purinergic signaling and intracellular communication via gap junctions, particularly in disease states such as MI.[46-48] Although the stellate ganglia serve as the primary efferent sympathetic outflow to the heart, its integrative and processing functions have been increasingly recognized.[49-51] For example, extracellular recordings of stellate ganglia activity identify greater network entropy and reduced neural specificity or synchrony with the cardiac cycle in a porcine

model with heart failure compared with controls.[51] In the present work, MI impaired sympathetically evoked changes in inotropy and lusitropy, which were rescued using cVNS, suggesting that cVNS may stabilize sympathetic function in disease states. Consistent with this, low level VNS in healthy canines increased stellate ganglia expression of small conductance calcium-activated potassium channels known to mediate afterhyperpolarizations, suggesting that cVNS may influence sympathetic nerve activity.[52] Myocardial ischemia also results in profound activation of spinal afferents in the high-thoracic DRG, the principal general visceral fibers innervating the heart.[53,54] Chronic activation of these afferents, partly mediated through transient receptor potential cation subfamily V member 1 channels, contributes to exaggerated sympatho-activation and adverse cardiac remodeling, whereas epicardial depletion of transient receptor potential cation subfamily V member 1 fibers attenuates remodeling after MI and improves cardiac function.[23,55] Using extracellular recording, Yoshie et al[23] found that depletion of these afferent fibers reduced sympathetic dysfunction after MI, suggesting interaction between spinal afferents and the stellate ganglia. Similarly, we found cVNS to reduce glial activation after MI in the DRG, which itself may explain in part the improved sympathetic function seen in MI + cVNS pigs compared with MI alone. Further work to understand spatiotemporal changes in sympathetic neuronal activity, as well as to elucidate primary vs secondary changes in the stellate ganglia and higher centers, is warranted.

CLINICAL PERSPECTIVE. A mechanistic and rationale basis of VNS therapy is imperative for appropriate clinical application in the setting of MI and heart failure.[9,20] Although low-intensity acute VNS is known to reduce the propensity for arrhythmias during experimentally induced coronary ischemia, the efficacy of cVNS therapy in experimental models is strongly influenced by stimulation parameters.[21] For example, Radcliffe et al[15] found no effect of cVNS therapy on pacing-induced cardiomyopathy in an ovine model when delivered at settings leading to a 30% bradycardia,[15] whereas Zhang et al[56] targeted a 10% bradycardia in a similar canine model and found attenuation of heart failure development, although VNS therapy was started earlier in their study. As demonstrated by our VNS titration protocol, increasing intensity of VNS initially evokes tachycardia followed by bradycardia; such an effect is consistent in dogs, pigs, and humans.[19,21,57] As such, dosing and delivery of VNS therapy, analogous to medications, has substantial impact on its efficacy and unintended off-target effects. Considerable differences in neural targets and stimulation parameters were evident in the 3 major trials of cVNS for reduced ejection heart failure.[16] The ANTHEM-HF (Autonomic Regulation Therapy to Enhance Myocardial Function in Heart Failure) trial operated at VNS parameters consistent with the neural fulcrum and led to improvements in both LV function and quality of life.[58-60] On the other hand, the VNS delivery modality and stimulation parameters for the 2 other major trials suffered from an inability to reach target VNS parameters due to side effects, which may partly explain the lack of clinical efficacy observed. Specifically, a post hoc analysis of the NECTAR-HF (Neural Cardiac Therapy For Heart Failure) trial, which found no improvement in LV function with cVNS, demonstrated that only 12% of the patients randomized to VNS therapy showed evidence for therapeutic engagement of the autonomic nervous system inputs to the heart.[61] The present work provides definitive evidence that cVNS exerts significant antiarrhythmic effects and mitigates aberrant cardiac and neural remodeling in large mammals when delivered in a rationale, neuroscience-guided manner. Such factors must be considered in further clinical trials of VNS or other device-based therapy.

STUDY LIMITATIONS. The present study has several limitations inherent to its design and defined objectives. We solely evaluated efficacy of right-sided VNS, which is the more commonly used modality in the clinical setting for treatment of cardiac pathologies. Pigs were titrated to neural fulcrum before MI for this study, which may not be feasible in the clinical setting. Further work will delineate the optimal time to initiate VNS, and fascicular stimulation may obviate the need for titration by avoiding off-target effects of VNS.[62] To demonstrate that our observed findings were mediated by cVNS after MI, rather than VNS-induced cardioprotection evolving from the titration phase, VNS was turned off before MI induction and not restarted until 2 days after MI. Furthermore, a group of animals, termed sham VNS + MI, were similarly titrated to neural fulcrum and underwent MI, but received no reactive VNS therapy after MI. Our sensitivity analysis clearly demonstrates that these animals were identical to MI alone with regard to myocardial performance, ventricular activation and repolarization properties, arrhythmia inducibility, and scar-border zone histologic characteristics (Supplemental Figure 2). In addition, our evaluation

of cardiac mechanical function was performed in the sedated state because echocardiography was not feasible in the conscious state in pigs. Among our cohort, 6 animals died within 48 h after MI due to SCD despite standard cardiopulmonary resuscitation. These animals were likely more susceptible to malignant VAs, and may have derived more substantial benefit from cVNS because prior studies have found greater impairment in parasympathetic function in animals susceptible to ischemia-induced arrhythmias compared with those resistant.[63,64] Further work is necessary to delineate the specific mechanisms by which cVNS imparts its cardioprotective effects, including its impact on neurotransmitter dynamics, scar-border zone properties, and remodeling of neural circuitry. In addition, studies investigating changes in biomarkers and heart rate variability with MI and cVNS may aid in clinical translation of this work.

CONCLUSIONS

Our data highlight that cVNS ameliorates myocardial structural and extracardiac neural remodeling that occurs early after MI, preventing heart failure. cVNS stabilizes the LV scar-border zone by reducing heterogeneity in activation and repolarization in vivo, drastically reducing the potential for lethal VAs. cVNS likewise improves sympathetic control of the heart post-MI, an effect that should result in a more robust reflex response to everyday cardiovascular stressors and translate into improved quality of life. These data suggest that restoration of parasympathetic function, whether pharmacologically or through neuromodulation, is an attractive therapeutic strategy for MI.

ACKNOWLEDGMENTS The authors acknowledge the donation of leads, implantable programmable generators, and programmers from LivaNova. We also acknowledge the technical assistance of Christopher Chan in these studies.

FUNDING SUPPORT AND AUTHOR DISCLOSURES

This work was supported by the National Institutes of Health through the Office of the Director Grant OT2 OD023848 (Drs Shivkumar, Ardell, Ajijola, and Hoover), the National Institute of Biomedical Imaging and Bioengineering Grant U01 EB025138 (Drs Shivkumar and Ardell), and the National Heart, Lung, and Blood Institute Grants F32 HL160163 (Dr Hadaya) and R01 HL159001 (Drs Ajijola, Shivkumar, and Ardell). University of California-Los Angeles has patents developed by Drs Ardell and Shivkumar relating to cardiac neural diagnostics and therapeutics. Drs Ardell, Ajijola, and Shivkumar are cofounders of NeuCures, Inc. All other authors have no relationships relevant to the contents of this paper to disclose.

ADDRESS FOR CORRESPONDENCE: Dr Jeffrey L. Ardell, UCLA Cardiac Arrhythmia Center and Neurocardiology Research Program of Excellence, David Geffen School of Medicine at UCLA, 100 Medical Plaza, Suite 660, Los Angeles, California 90095, USA. E-mail: JArdell@mednet.ucla.edu. OR Dr Kalyanam Shivkumar, UCLA Cardiac Arrhythmia Center and Neurocardiology Research Program of Excellence, David Geffen School of Medicine at UCLA, 100 Medical Plaza, Suite 660, Los Angeles, California 90095, USA. E-mail: KShivkumar@mednet.ucla.edu.

PERSPECTIVES

COMPETENCY IN MEDICAL KNOWLEDGE: Neurohormonal remodeling after MI is characterized by chronic sympatho-excitation, which, although initially helping to maintain cardiac output, ultimately becomes maladaptive and contributes to the risk of death. VNS has emerged as a promising therapeutic approach to combat the observed withdrawal of parasympathetic tone and to counteract the reflex-mediated sympathoexcitation associated with ischemic heart disease. Reactive cVNS, delivered in a neurophysiological-guided manner, maintains autonomic and cardiac mechanical function while stabilizing the LV scar-border zone by reducing heterogeneities in both activation and repolarization in vivo, drastically reducing the potential for VT /VF.

TRANSLATIONAL OUTLOOK: The translatability of cVNS for cardiovascular disease has been hampered by a lack of knowledge regarding cardiac reflexes, cardiac and extracardiac remodeling that occurs during disease, and appropriate delivery of VNS therapy. The present work provides definitive evidence that cVNS, delivered in a neurophysiological-guided manner, exerts significant antiarrhythmic effects, and mitigates aberrant cardiac and neural remodeling in large mammals when delivered in a rationale, neurophysiological-guided manner. Such factors must be considered in further clinical trials of VNS or other device-based therapy.

REFERENCES

1. Stecker EC, Reinier K, Marijon E, et al. Public health burden of sudden cardiac death in the United States. *Circ Arrhyth Electrophysiol*. 2014;7:212–217.

2. Benjamin EJ, Virani SS, Callaway CW, et al. American Heart Association Council on Epidemiology and Prevention Statistics Committee and Stroke Statistics Subcommittee. Heart disease and stroke statistics-2018 update: a report from the American Heart Association. *Circulation*. 2018;137:e67–e492.

3. Ardell JL, Andresen MC, Armour JA, et al. Translational neurocardiology: preclinical models and cardioneural integrative aspects. *J Physiol*. 2016;594:3877–3909.

4. Fukuda K, Kanazawa H, Aizawa Y, Ardell JL, Shivkumar K. Cardiac innervation and sudden cardiac death. *Circ Res*. 2015;116:2005–2019.

5. Ibanez B, James S, Agewall S, et al. 2017 ESC Guidelines for the management of acute myocardial infarction in patients presenting with ST-segment elevation: the Task Force for the management of acute myocardial infarction in patients presenting with ST-segment elevation of the European Society of Cardiology (ESC). *Eur Heart J*. 2018;39:119–177.

6. O'Gara PT, Kushner FG, Ascheim DD, et al. American College of Cardiology Foundation/American Heart Association Task Force on Practice Guidelines. 2013 ACCF/AHA guideline for the management of ST-elevation myocardial infarction: a report of the American College of Cardiology Foundation/American Heart Association Task Force on Practice Guidelines. *J Am Coll Cardiol*. 2013;61(4):e78–e140.

7. Schwartz PJ, La Rovere MT, Vanoli E. Autonomic nervous system and sudden cardiac death. Experimental basis and clinical observations for post-myocardial infarction risk stratification. *Circulation*. 1992;85(1 Suppl):I77–I191.

8. La Rovere MT, Bigger JT Jr, Marcus FI, Mortara A, Schwartz PJ. Baroreflex sensitivity and heart-rate variability in prediction of total cardiac mortality after myocardial infarction. ATRAMI (Autonomic Tone and Reflexes After Myocardial Infarction) Investigators. *Lancet*. 1998;351:478–484.

9. Shivkumar K, Ajijola OA, Anand I, et al. Clinical neurocardiology defining the value of neuroscience-based cardiovascular therapeutics. *J Physiol*. 2016;594:3911–3954.

10. Waxman MB, Wald RW. Termination of ventricular tachycardia by an increase in cardiac vagal drive. *Circulation*. 1977;56:385–391.

11. Ando M, Katare RG, Kakinuma Y, et al. Efferent vagal nerve stimulation protects heart against ischemia-induced arrhythmias by preserving connexin43 protein. *Circulation*. 2005;112:164–170.

12. Beaumont E, Southerland EM, Hardwick JC, et al. Vagus nerve stimulation mitigates intrinsic cardiac neuronal and adverse myocyte remodeling postmyocardial infarction. *Am J Physiol Heart Circulatory Physiol*. 2015;309:H1198–H1206.

13. Li M, Zheng C, Sato T, Kawada T, Sugimachi M, Sunagawa K. Vagal nerve stimulation markedly improves long-term survival after chronic heart failure in rats. *Circulation*. 2004;109(1):120–124.

14. Hamann JJ, Ruble SB, Stolen C, et al. Vagus nerve stimulation improves left ventricular function in a canine model of chronic heart failure. *Eur J Heart Fail*. 2013;15:1319–1326.

15. Radcliffe EJ, Pearman CM, Watkins A, et al. Chronic vagal nerve stimulation has no effect on tachycardia-induced heart failure progression or excitation-contraction coupling. *Physiological Rep*. 2020;8:e14321. https://doi.org/10.14814/phy2.14321

16. Anand IS, Konstam MA, Klein HU, et al. Comparison of symptomatic and functional responses to vagus nerve stimulation in ANTHEM-HF, INOVATE-HF, and NECTAR-HF. *ESC Heart Fail*. 2020;7:75–83.

17. Gold MR, Van Veldhuisen DJ, Hauptman PJ, et al. Vagus nerve stimulation for the treatment of heart failure: the INOVATE-HF trial. *J Am Coll Cardiol*. 2016;68:149–158.

18. Zannad F, De Ferrari GM, Tuinenburg AE, et al. Chronic vagal stimulation for the treatment of low ejection fraction heart failure: results of the NEural Cardiac TherApy foR Heart Failure (NECTAR-HF) randomized controlled trial. *Eur Heart J*. 2015;36:425–433.

19. Premchand RK, Sharma K, Mittal S, et al. Autonomic regulation therapy via left or right cervical vagus nerve stimulation in patients with chronic heart failure: results of the ANTHEM-HF trial. *J Cardiac Fail*. 2014;20:808–816.

20. Hadaya J, Ardell JL. Autonomic modulation for cardiovascular disease. *Front Physiol*. 2020;11:617459.

21. Ardell JL, Nier H, Hammer M, et al. Defining the neural fulcrum for chronic vagus nerve stimulation: implications for integrated cardiac control. *J Physiol*. 2017;595:6887–6903.

22. Beaumont E, Wright GL, Southerland EM, et al. Vagus nerve stimulation mitigates intrinsic cardiac neuronal remodeling and cardiac hypertrophy induced by chronic pressure overload in guinea pig. *Am J Physiol Heart Circulatory Physiol*. 2016;310:H1349–H1359.

23. Yoshie K, Rajendran PS, Massoud L, et al. Cardiac TRPV1 afferent signaling promotes arrhythmogenic ventricular remodeling after myocardial infarction. *JCI Insight*. 2020;5:1–13.

24. Buckley U, Chui RW, Rajendran PS, Vrabec T, Shivkumar K, Ardell JL. Bioelectronic neuromodulation of the paravertebral cardiac efferent sympathetic outflow and its effect on ventricular electrical indices. *Heart Rhythm*. 2017;14:1063–1070.

25. Schindelin J, Arganda-Carreras I, Frise E, et al. Fiji: an open-source platform for biological-image analysis. *Nat Methods*. 2012;9:676–682.

26. Rivaud MR, Bayer JD, Cluitmans M, et al. Critical repolarization gradients determine the induction of reentry-based torsades de pointes arrhythmia in models of long QT syndrome. *Heart Rhythm*. 2021;18:278–287.

27. Haws CW, Lux RL. Correlation between in vivo transmembrane action potential durations and activation-recovery intervals from electrograms. Effects of interventions that alter repolarization time. *Circulation*. 1990;81:281–288.

28. Salavatian S, Beaumont E, Longpre JP, et al. Vagal stimulation targets select populations of intrinsic cardiac neurons to control neurally induced atrial fibrillation. *Am J Physiol Heart Circulatory Physiol*. 2016;311:H1311–H1320.

29. Chauhan VS, Downar E, Nanthakumar K, et al. Increased ventricular repolarization heterogeneity in patients with ventricular arrhythmia vulnerability and cardiomyopathy: a human in vivo study. *Am J Physiol Heart Circulatory Physiol*. 2006;290:H79–H86.

30. Janse MJ, Coronel R, Opthof T, Sosunov EA, Anyukhovsky EP, Rosen MR. Repolarization gradients in the intact heart: transmural or apicobasal? *Prog Biophys Mol Biol*. 2012;109:6–15.

31. Ajijola OA, Yagishita D, Reddy NK, et al. Remodeling of stellate ganglion neurons after spatially targeted myocardial infarction: neuropeptide and morphologic changes. *Heart Rhythm*. 2015;12:1027–1035.

32. Ajijola OA, Hoover DB, Simerly TM, et al. Inflammation, oxidative stress, and glial cell activation characterize stellate ganglia from humans with electrical storm. *JCI Insight*. 2017;2:1–11.

33. Vanoli E, De Ferrari GM, Stramba-Badiale M, Hull SS Jr, Foreman RD, Schwartz PJ. Vagal stimulation and prevention of sudden death in conscious dogs with a healed myocardial infarction. *Circ Res*. 1991;68:1471–1481.

34. Shinlapawittayatorn K, Chinda K, Palee S, et al. Vagus nerve stimulation initiated late during ischemia, but not reperfusion, exerts cardioprotection via amelioration of cardiac mitochondrial dysfunction. *Heart Rhythm*. 2014;11:2278–2287.

35. Shinlapawittayatorn K, Chinda K, Palee S, et al. Low-amplitude, left vagus nerve stimulation significantly attenuates ventricular dysfunction and infarct size through prevention of mitochondrial dysfunction during acute ischemia-reperfusion injury. *Heart Rhythm*. 2013;10:1700–1707.

36. Machhada A, Hosford PS, Dyson A, Ackland GL, Mastitskaya S, Gourine AV. Optogenetic stimulation of vagal efferent activity preserves left ventricular function in experimental heart failure. *J Am Coll Cardiol Basic Trans Sci*. 2020;5:799–810.

37. Seki A, Fishbein MC. Ischemic heart disease. In: McManus LM, Mitchell RN, eds. *Pathobiology of Human Disease*. Academic Press; 2014:995–1013.

38. Adegboyega PA, Haque AK, Boor PJ. Extensive myocytolysis as a marker of sudden cardiac death. *Cardiovasc Pathol*. 1996;5:315–321.

39. De Ferrari GM, Vanoli E, Stramba-Badiale M, Hull SS Jr, Foreman RD, Schwartz PJ. Vagal

reflexes and survival during acute myocardial ischemia in conscious dogs with healed myocardial infarction. *Am J Physiol*. 1991;261:H63–H69.

40. Malliani A, Recordati G, Schwartz PJ. Nervous activity of afferent cardiac sympathetic fibres with atrial and ventricular endings. *J Physiol*. 1973;229:457–469.

41. Hoover DB, Shepherd AV, Southerland EM, Armour JA, Ardell JL. Neurochemical diversity of afferent neurons that transduce sensory signals from dog ventricular myocardium. *Autonom Neurosci Basic Clin*. 2008;141:38–45.

42. Nakamura K, Ajijola OA, Aliotta E, Armour JA, Ardell JL, Shivkumar K. Pathological effects of chronic myocardial infarction on peripheral neurons mediating cardiac neurotransmission. *Autonom Neurosci Basic Clin*. 2016;197:34–40.

43. Wang L, Olivas A, Francis Stuart SD, et al. Cardiac sympathetic nerve transdifferentiation reduces action potential heterogeneity after myocardial infarction. *Am J Physiol Heart Circulatory Physiol*. 2020;318:H558–H565.

44. Kanazawa H, Ieda M, Kimura K, et al. Heart failure causes cholinergic transdifferentiation of cardiac sympathetic nerves via gp130-signaling cytokines in rodents. *J Clin Invest*. 2010;120:408–421.

45. Olivas A, Gardner RT, Wang L, Ripplinger CM, Woodward WR, Habecker BA. Myocardial infarction causes transient cholinergic transdifferentiation of cardiac sympathetic nerves via gp130. *J Neurosci*. 2016;36:479–488.

46. van Weperen VYH, Littman RJ, Arneson DV, Contreras J, Yang X, Ajijola OA. Single-cell transcriptomic profiling of satellite glial cells in stellate ganglia reveals developmental and functional axial dynamics. *Glia*. 2021;69:1281–1291.

47. Feldman-Goriachnik R, Hanani M. The effects of sympathetic nerve damage on satellite glial cells in the mouse superior cervical ganglion. *Autonom Neurosci Basic Clin*. 2019;221:102584.

48. Shao LJ, Liang SD, Li GL, Xu CS, Zhang CP. Exploration of P2X3 in the rat stellate ganglia after myocardial ischemia. *Acta Histochem*. 2007;109:330–337.

49. Gurel NZ, Sudarshan KB, Tam S, et al. Studying cardiac neural network dynamics: challenges and opportunities for scientific computing. *Front Physiol*. 2022;13:835761.

50. Sudarshan KB, Hori Y, Swid MA, et al. A novel metric linking stellate ganglion neuronal population dynamics to cardiopulmonary physiology. *Am J Physiol Heart Circulatory Physiol*. 2021;321:H369–H381.

51. Gurel NZ, Sudarshan KB, Hadaya J, et al. Metrics of high conflictuation and entropy to describe control of cardiac function in the stellate ganglia. *bioRxixorg*. 2021, 2021.09.28.462183v4.

52. Shen MJ, Hao-Che C, Park HW, et al. Low-level vagus nerve stimulation upregulates small conductance calcium-activated potassium channels in the stellate ganglion. *Heart Rhythm*. 2013;10:910–915.

53. Salavatian S, Ardell SM, Hammer M, Gibbons DD, Armour JA, Ardell JL. Thoracic spinal cord neuromodulation obtunds dorsal root ganglion afferent neuronal transduction of the ischemic ventricle. *Am J Physiol Heart Circulatory Physiol*. 2019;317(5):H1134–H1141.

54. Armour JA, Linderoth B, Arora RC, et al. Long-term modulation of the intrinsic cardiac nervous system by spinal cord neurons in normal and ischaemic hearts. *Autonomic Neurosci Basic Clin*. 2002;95:71–79.

55. Wang HJ, Wang W, Cornish KG, Rozanski GJ, Zucker IH. Cardiac sympathetic afferent denervation attenuates cardiac remodeling and improves cardiovascular dysfunction in rats with heart failure. *Hypertension*. 2014;64:745–755.

56. Zhang Y, Popovic ZB, Bibevski S, et al. Chronic vagus nerve stimulation improves autonomic control and attenuates systemic inflammation and heart failure progression in a canine high-rate pacing model. *Circ Heart Fail*. 2009;2:692–699.

57. Nearing BD, Libbus I, Amurthur B, Kenknight BH, Verrier RL. Acute autonomic engagement assessed by heart rate dynamics during vagus nerve stimulation in patients with heart failure in the ANTHEM-HF Trial. *J Cardiovasc Electrophysiol*. 2016;27:1072–1077.

58. Premchand RK, Sharma K, Mittal S, et al. Extended follow-up of patients with heart failure receiving autonomic regulation therapy in the ANTHEM-HF study. *J Cardiac Fail*. 2016;22:639–642.

59. Sharma K, Premchand RK, Mittal S, et al. Long-term follow-up of patients with heart failure and reduced ejection fraction receiving autonomic regulation therapy in the ANTHEM-HF Pilot Study. *Int J Cardiol*. 2021;323:175–178.

60. Konstam MA, Udelson JE, Butler J, et al. Impact of autonomic regulation therapy in patients with heart failure: ANTHEM-HFrEF pivotal study design. *Circ Heart Fail*. 2019;12:e005879.

61. De Ferrari GM, Stolen C, Tuinenburg AE, et al. Long-term vagal stimulation for heart failure: eighteen month results from the NEural Cardiac TherApy foR Heart Failure (NECTAR-HF) trial. *Int J Cardiol*. 2017;244:229–234.

62. Fitchett A, Mastitskaya S, Aristovich K. Selective neuromodulation of the vagus nerve. *Front Neurosci*. 2021;15:685872.

63. Billman GE. A comprehensive review and analysis of 25 years of data from an in vivo canine model of sudden cardiac death: implications for future anti-arrhythmic drug development. *Pharmacol Therapeut*. 2006;111:808–835.

64. Collins MN, Billman GE. Autonomic response to coronary occlusion in animals susceptible to ventricular fibrillation. *Am J Physiol*. 1989;257:H1886–H1894.

KEY WORDS myocardial infarction, neurocardiology, sympathetic nervous system, vagal nerve stimulation, ventricular tachycardia/ventricular fibrillation

APPENDIX For supplemental tables and figures, please see the online version of this paper.